Statistical Tests for the Comparison of Surface Gravity Wave Spectra with Application to Model Validation

A. GUILLAUME

Météorologie Nationale, Paris, France

(Manuscript received 30 August 1989, in final form 7 February 1990)

ABSTRACT

A new second generation deep-water ocean wave model VAG is presented and several modifications are tested on a one month hindcast. On the same period and with the same windfields a version of the third generation model WAM is also tested. All the results are compared with the data of a pitch-roll-heave buoy moored at the entrance of the English Channel in 110 meters depth. This necessitates a preliminary investigation of existing tools to carry such comparisons. Based on commonly used criteria in model testing VAG and WAM achieve similar results. New tests are defined. For the significant wave heights, the use of the scatter index is criticized and the notion of relative error is introduced. For the mean wave directions, a weighted mean angular gap is defined which minimizes the impact of the direction errors of the low waves. From the theory of stationary random processes applied to waves, a criterion is proposed for frequency spectrum comparisons. Some diagrams are designed for the comparisons of more directional information. The sensitivity of the new tests to small differences in the modeling of the spectra attests to their suitability for model comparisons. Their application to the various runs shows that 1) In VAG, the swell modeling is improved by reducing the directional resolution of the spectrum and the grid mesh size. A reshaping of the windsea with a f^{-4} power law for the high frequencies gives better results. 2) Swells are better modeled with WAM. 3) For both models, the direction of the high waves are better predicted. 4) In wind turning situations, a lag time between wind turning and wave turning is observed by the buoy even for rather high frequency waves. This lag time is correctly reproduced with VAG, but is too long with WAM.

1. Introduction

VAG is a new second generation ocean wave model that is now operational at the "Météorologie Nationale" where it has replaced the DSA5 first generation model (Gelci-Devillaz 1969) for the North Atlantic marine forecast. Its early development has followed the method developed by Golding for the British Meteorological Office model (BMO), as published in 1983 (Golding 1983). Several modifications have been introduced to overcome some of the difficulties highlighted during the SWAMP intercomparison of wave models (The SWAMP Group 1985), especially in wind turning situations. Our approach is different from the one followed meanwhile by BMO (Ephraums, personal communication) and is based on a new scheme for the determination of the windsea part of the spectrum in which the nonlinear energy transfers are considered. The nonlinear interactions are conducted in this part of the spectrum by redistributing the energy to lead to a JONSWAP spectrum whose parameters are all derived from the value of the total windsea energy. The model is fully described in Guillaume (1987), where tests, first with the SWAMP cases (The SWAMP Group 1985), and then against available weather ship observations for a one-month hindcast study are reported. An improvement over the previous model DSA5 is shown, but the quality of the data is found insufficient to fully assess the performances of the model.

Taking advantage of the directional data recorded by the buoy "BEATRICE," moored at the entrance of the Channel in 110 meters depth, and provided by the "Service Technique des Phares et Balises," the hindcast study has focused on comparisons with these data and some modifications in VAG have been tried. They include an increase of the directional resolution of the wave spectrum and some grid modifications, in relation with swell propagation problems suspected by Guillaume (1987), a reduction of the second order propagation scheme to a first order, for operational outlook of saving computer resources, and a modified windsea parameterization based on results obtained by Donelan et al. (1985).

A hindcast done within the WAM project (Komen 1985) with the version WAMD1 of the third generation model WAM (WAM Development and Implementation Group 1988) widens the comparison study to a model of different structure. The nonlinear transfers are fully introduced in the energy balance equation

Corresponding author address: Dr. A. Guillaume, Ministère des Transports et de la Mer, Direction de la Meteorologie Nationale, Service Central d'Exploitation de la Météorologie, 2, Avenue Rapp-75340, Paris, Cedex 07, France.

and calculated without making any assumption on the shape of the spectrum. The great interest of this run is that it is done for the same area and with the same windfields already chosen for testing VAG. These windfields are issued from the atmospheric model of the European Centre for Medium Range Weather Forecasts. Analyzed fields that integrate all available routine observations are chosen and the wave models are run with a similar spatial resolution as the atmospheric model, which minimizes interpolation and scale effects.

The great number of model results to compare with the data necessitates proper tools to carry comparisons. The wealth of the data, together with the quality of the concomitant ECMWF windfields, provides a robust background to analyze the performances of such existing tools. A need to improve them emerges. Moreover, the wealth of the data motivates the definition of new ones. More precisely, from the structure of both types of information, model output and observed data, a set of comparable quantities is first derived. Their values are computed for all the runs and for the buoy, and are gathered in a database from which all the quantities to be compared are obtained. They are first the significant wave height and the mean wave direction for which some new statistical parameters are introduced. Frequency spectra are next computed and a criterion is defined to compare them. Its definition is based on the application of the theory of stationary random processes to waves (Pierson 1955; Neumann-Pierson 1966). It quantifies in terms of probability the ability of the model to give the true spectrum of which one observation is given by the buoy. It is a function of the frequency and the following hypotheses are made: 1) The instrumental errors are negligible compared with model ones. 2) Within a frequency bin of the model the true spectrum is slowly varying. Finally, diagrams to plot more directional information included in the database are designed.

These tools are then applied to the analysis of the results obtained by the various models. This includes a discussion of their ability to highlight the models' behavior differences.

The paper is organized as follows. The VAG model is described in section 2, and the buoy data in section 3. Section 4 presents the tests done with the VAG model and the WAM run. All the definitions for the comparison study are presented in section 5. Section 6 gives the results.

2. VAG: Second generation wave prediction model

According to the SWAMP terminology (The SWAMP Group 1985), VAG is a second generation coupled discrete model. A full description of the model is given in Guillaume (1987).

Briefly, the deep water version tested here is based on the energy balance equation

$$\partial E/\partial t + v \cdot \mathrm{grad}(E) = S = S_{\mathrm{in}} - S_{\mathrm{ds}} + S_{\mathrm{nl}}, \quad (2.1)$$

where $E(f, \theta)$, the directional wave spectrum, is related to the sea-surface elevation ζ by

$$\iint E(f, \theta) df d\theta = \langle \overline{\zeta^2} \rangle^* \quad (2.2)$$

and v is the group velocity ($v = g/4\pi f$ in deep water).

Here S, the source term, includes the wind input S_{in}, the dissipation S_{ds}, and the nonlinear interactions S_{nl}.

a. *Physical aspects of the model*

The wind input is described by

$$S_{\mathrm{in}} = A + B \cdot E(f, \theta). \quad (2.3)$$

For the linear growth, the following expression adapted from Golding (1983) is chosen

$$A = \begin{cases} A_1 \cdot U^2 \cdot G(\theta - \phi), & \text{for} \quad f = f_{\max} \\ 0, & \text{otherwise} \end{cases} \quad (2.4)$$

$f_{\max}$ is the highest frequency used by the model and, at this stage, is the only one affected by the linear input: the energy will be redistributed afterwards by the nonlinear interactions treatment. Here U is the wind speed at 10 meters, ϕ the wind direction, and G the cosine squared spreading function,

$$G(\theta - \phi) = \begin{cases} 2\cos^2(\theta - \phi)/\pi, & \text{for} \quad |\theta - \phi| < \pi/2 \\ 0, & \text{otherwise} \end{cases} \quad (2.5)$$

A_1 is a tuned coefficient, adjusted to $A_1 = 0.49 \times 10^{-6}/f_{\max}$.

The exponential growth coefficient B follows the classical expression already used by Barnett (1968), Golding (1983), and more recently in the WAM model (WAM 1988)

$$B = \begin{cases} B_1 \cdot 2\pi f \rho \cdot [U \cos(\theta - \phi)/c - 1], \\ \quad \text{for} \quad [U \cos(\theta - \phi)/c - 1] > 0 \\ 0, \quad \text{otherwise} \end{cases} \quad (2.6)$$

c is the phase speed, $c = g/2\pi f$ in deep water, where ρ is the ratio of the air density to the water density, $\rho = 1.2/1033$, and B_1 is adjusted by tuning to 0.054 and is very close to the value proposed by Golding (1983), but quite different from the one used in WAM which is based on measurements by Snyder et al. (1981).

The dissipation is based on the theoretical work of Hasselmann (1974) and is given by

---

* Whenever used integrals in θ, are from 0 to 2π, and integrals in f, from 0 to infinity.

$$S_{ds} = \Phi(E) f^2 E(f, \theta) \quad (2.7)$$

with $\Phi(E)$ depending on the total energy E_T,

$$E_T = \iint E(f, \theta) df d\theta \quad (2.8)$$

and adjusted, as suggested by Golding to

$$\Phi(E) = 1.25 \times 10^{-3} (E_T/g^2)^{1/4}. \quad (2.9)$$

Moreover, the growth is limited. The total wind–sea energy, as further defined, remains smaller than the total energy of the Pierson–Moskowitz spectrum for the local wind,

$$E_{PMT} = 0.0036 U^4 g^{-2}. \quad (2.10)$$

The nonlinear interactions are taken into account by splitting the spectrum in two parts, wind sea and swell, and by reshaping the windsea part in a JONSWAP spectrum

$$E_{JSP}(f) = \alpha g^2 (2\pi)^{-4} f^{-5} \exp[-1.25(f/f_p)^{-4}] \gamma^J \quad (2.11)$$

with

$$J = \exp[-(f - f_p)^2 / 2\sigma^2 f_p^2] \quad (2.12)$$

and using the cosine squared spreading function G. The four parameters α, f_p, γ, and σ are defined below. The splitting between wind sea and swell is done after wind input and dissipation. The basic idea is to consider windsea as being the spectral bins of direction less than 90 degrees each side of the local wind direction, and of frequency higher than a minimum value $f_{min}(\theta)$, depending on the angle from the wind $|\theta - \phi|$. The total windsea energy, E_{WST}, is then given by

$$E_{WST} = \int_{|\theta - \phi| < 90} \left[\int_{f > f_{min}(\theta)} E(f, \theta) df \right] d\theta. \quad (2.13)$$

where $f_{min}(\theta)$ is obtained by an iterative process, starting from a value that can be considered as the lowest possible one:

$$f_{min}(\theta) = 0.8 f_{PM}(\theta) \quad (2.14)$$

with

$$f_{PM}(\theta) = 0.13 g/U \cos(\theta - \phi). \quad (2.15)$$

Here $f_{PM}(\theta)$ is the peak frequency of a Pierson–Moskowitz (PM) spectrum corresponding to the part of the local wind in the direction of the involved wave. The 0.8 coefficient is there to include the forward face of the spectrum. Equation (2.14) is rewritten

$$f_{min}(\theta) = 0.8 f_P / \cos(\theta - \phi) \quad (2.16)$$

and this structure is kept in the following, while focusing on the determination of f_P. Its first value is thus $f_P = 0.13 g/U$. Thereby, (2.13) provides a first approximation of E_{WST} which is used in the growth limitation. A second approximation of f_P is then obtained by

$$f_P = 0.032 (E_{WST})^{-1/4} g^{1/2} \quad (2.17)$$

which is the inversion of the relation existing, for a PM spectrum, between its total energy and its peak value. This leads to a second approximation of E_{WST} from which the final value of f_P is inferred, using results from the JONSWAP experiment and given by equation (3.6) of Hasselmann (1976) equivalent to

$$f_P = f_{PM} (E_{WST}/E_{PMT})^{-3/10}. \quad (2.18)$$

The JONSWAP parameters are then obtained by

$$f_p = f_P,$$

$$\gamma = 3.3 - 2.3 (E_{WST}/E_{PMT})^2, \quad (2.19)$$

an adjustment proposed by Golding (1983) and based on the JONSWAP Experiment (1973). The shape parameter σ is set to 0.08, the mean value observed during the JONSWAP Experiment.

In the JONSWAP spectrum, the rear face of the spectrum is described by a f^{-5} power law, which has been called into question by many authors in recent years (Kitaïgorodskii et al. 1975; Mitsuyasu et al. 1975; Foristall 1981). Recent work by Donelan et al. (1985) shows that a f^{-4} power law gives a better description in the energy containing region, of main interest for the model, and suggests the use of a modified JONSWAP spectrum

$$E_{JSPM}(f) = \alpha g^2 (2\pi)^{-4} f^{-4} f_p^{-1} \exp[(f/f_p)^{-4}] \gamma^J,$$

J given by (2.12). (2.20)

Adjustments are proposed for the enhancement factor γ and the shape parameter σ in terms of U_c/c_p ratio of the component of the wind speed in the direction of the waves at the peak of the spectrum to the phase speed of those waves. This ratio reduces to U/c_p in VAG because the windsea is adjusted symmetrically to the wind direction and their formulae become:

$$\gamma = \begin{cases} 1.7, & 0.83 < U/c_p < 1 \\ 1.7 + 6.0 \text{ Log}(U/c_p), & 1 \leqslant U/c_p < 5 \end{cases} \quad (2.21)$$

and

$$\sigma = 0.08[1 + 4/(U/c_p)^3] \quad 0.83 < U/c_p < 5. \quad (2.22)$$

This is tested in one of the runs but with a cosine squared distribution, and not with the distribution these authors proposed.

b. *Numerical aspects of the model*

The model VAG uses a stereographic grid. For the integration of the source term, a first order explicit scheme is implemented. For the advection term, a sec-

ond order explicit Lax–Wendroff scheme, in its version modified by Gadd (1978), is used. In one of the tests, it is replaced by a first order upstream propagation scheme defined by

$$E^{n+1}_{i,j} = E^n_{i,j} - \mu_x(E^n_{i,j} - E^n_{i-\epsilon,j}) - \mu_y(E^n_{i,j} - E^n_{i,j-\epsilon'}) \quad (2.23)$$

where $\mu_x = v(\cos\theta)\Delta t/\Delta x$, $\mu_y = v(\sin\theta)\Delta t/\Delta y$, $\epsilon = \text{sign}(\mu_x)$, $\epsilon' = \text{sign}(\mu_y)$. Here Δt is the time step, $(\Delta x, \Delta y)$ the mesh size, which depends on its localization in the grid, and

$$E^n_{i,j} = E(n\Delta t, i\Delta x, j\Delta y).$$

An important aspect of the model is its modular structure. Namely, two main tasks are isolated, VAGACR for the source term, the VAGADV for the propagation. An initialization routine sets up the characteristics of the model: frequency discretization, directional resolution, wind precision, and grid specification such as location, mesh, and coastlines. All these parameters are adjustable, together with the coastlines which are first settled using the US Navy Summary, and then manually adaptable.

3. The buoy "BEATRICE"

This section describes the data provided by the "Service Technique des Phares et Balises." These data are processed from the observations of the pitch–roll–heave sensor of the buoy "BEATRICE" (Bouée-phare: Equipement d'Acquisition de Traitement et de Restitution d'Information de Comportement et d'Environnement, Racapé 1986, 1987). This buoy is moored at the entrance of the English Channel, offshore Ushant, 48°31′42″ N and 5°49′03″ W, in 110 meters depth.

The information about the directional spectrum are obtained by the method developed and implemented by Ezraty et al. (1981, 1983), which is based on the theoretical work of Longuet-Higgins (1963). From the records of the vertical displacement ζ and of the angles of pitching and rolling, the three quantities

$$\xi_1 = \zeta, \quad \xi_2 = \partial\zeta/\partial x, \quad \xi_3 = \partial\zeta/\partial y \quad (3.1)$$

are available. It is then possible to estimate the cospectra $C_{i,j}$ and quadspectra $Q_{i,j}$ of any pair (ξ_i, ξ_j) by fast Fourier transform, and therefrom the first five coefficients of the Fourier development of the spectrum in

$$E(f,\theta) = A_0(f) + A_1(f)\cos[\theta - \theta_1(f)] + A_2(f)\cos[2(\theta - \theta_2(f)] + \cdots \quad (3.2)$$

These are given by

$$A_0(f) = C_{1,1}/2\pi$$
$$A_1(f)\cos[\theta_1(f)] = Q_{1,2}/k\pi,$$
$$A_1(f)\sin[\theta_1(f)] = Q_{1,3}/k\pi$$
$$A_2(f)\cos[2\theta_2(f)] = (C_{2,2} - C_{3,3})/k^2\pi,$$
$$A_2(f)\sin[2\theta_2(f)] = 2C_{2,3}/k^2\pi, \quad (3.3)$$

where k is the wavenumber, and satisfies the dispersion relation in deep water,

$$gk = (2\pi f)^2. \quad (3.4)$$

As k is independent of θ, whatever may be the shape of the spectrum, $\theta_1(f)$ is related to the directional spectrum by

$$\theta_1(f) = \arg\left[\int E(f,\theta)\exp(i\theta)d\theta\right]. \quad (3.5)$$

The data provided consist in the mean directions $\theta_1(f)$ and the energy densities $E(f) = A_0(f)$, for 64 frequencies ranging from 1/128 to 0.5 Hz. They are obtained from signals recorded to a frequency of 2 Hz and the length of the records is of 2048 seconds (34 min, 8 s).

4. Description of the models' runs

Taking the opportunity of a flexible tool, several versions of the VAG model have been tested. In the last section, results obtained with the five following ones are presented. They have been selected because they show various aspects of the model and also allow a better understanding of the statistical tools presented in the section 5.

- VAG12: It is the original version. The spectra have 12 directions of propagation ($\Delta\theta = 30°$) and 12 frequencies starting from 0.04 Hz with an increment $\Delta f/f = 0.2$. The grid is polar stereographic, with the Greenwich meridian as reference, and has a 150 km mesh size at 60°N (Fig. 1). For the propagation, the second-order Lax-Wendroff scheme is implemented

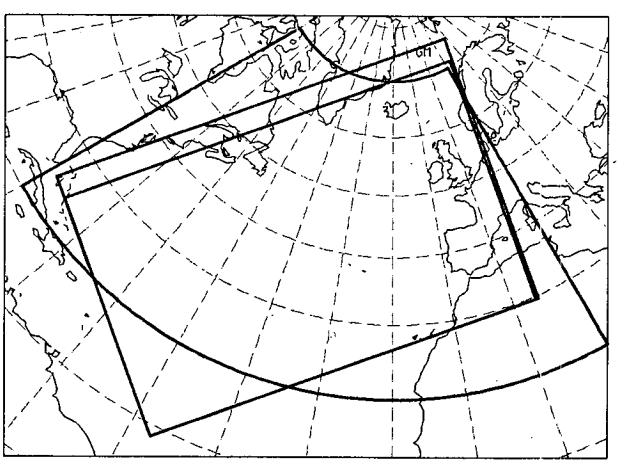

FIG. 1. Coverage of the grids used during the tests: (W) regular latitude/longitude, 1° × 1°; (V1) polar stereographic, 150 km at 60°N; (V2) polar stereographic, 100 km at 60°N.

TABLE 1. The main characteristics of the runs.

Run	Grid characteristics	Direction nb ($\Delta\theta$)	Frequency nb (range)	Propagation scheme	Windsea spectrum
VAG12	stereo.150 km	12 (30°)	12 (.04/0.3)	Lax-W 2	Jonswap
VAG18	stereo.150 km	18 (20°)	12 (.04/0.3)	Lax-W 2	Jonswap
VAGAD1	stereo.150 km	18 (20°)	12 (.04/0.3)	Upstr. 1	Jonswap
VAGDO	stereo.150 km	18 (20°)	12 (.04/0.3)	Lax-W 2	Jons. + Donelan
VAGG2	stereo.100 km	18 (20°)	12 (.04/0.3)	Lax-W 2	Jonswap
WAM	lat/long 1° × 1°	12 (30°)	26 (.04/0.45)	Upstr. 1	no restriction

and the reshaping of the windsea is in the JONSWAP spectrum E_{JSP} (2.11).

- VAG18: the directional resolution of the spectra is increased from 12 to 18 directions to investigate the underestimation of significant wave height in swell dominated situations reported in Guillaume (1987). This high resolution is kept for all the following tests.
- VAGG2: In Guillaume (1987), it is also suspected that the limitation of the grid to the north could explain some of the swell underestimations noticed. The grid is widened to the north (Fig. 1). The grid mesh size is decreased to 100 km at 60°N to go closer to the resolution used in the WAM run.
- VAGAD1: The first order propagation scheme described in section 2b is implemented to justify operational computer resources.
- VAGDO: The windsea is reshaped in the modified Jonswap spectrum E_{JSPM} (2.20), with a cosine squared spreading function. The initial Lax Wendroff scheme is used.

The WAM run has been done with the WAMD1 version of the third generation model, made available on the CRAY-XMP of the European Centre for Medium Range Weather Forecasts (Hasselmann 1987). It has the following characteristics:

- WAM: The spectra have 12 directions of propagation and 26 frequencies starting from 0.042 with an increment $\Delta f/f$ of 1.1. The grid is a regular lat./long. grid of resolution one degree × one degree. It covers an area from 20° to 70°N and 80°W to 10°E (Fig. 1). The mesh size at 60°N is then 55 km × 110 km. The propagation is done with a first order explicit scheme.

A summary of the main differences of all the runs is given in Table 1. All runs have been done on the CRAY-XMP of the European Centre for Medium Range Weather Forecasts, with the 10 meter analyzed windfields obtained from their archives, for the period 5 November 1985 to 5 December 1985, starting with a background situation. For the winds, a specific interpolation routine is incorporated in the WAM system (Hasselmann 1987). The first two days, used to warm up the model, are discarded. Outputs are collected every six hours, at the main synoptic hours 0000, 0600, 1200, and 1800 UTC.

5. Tools for comparison with pitch-roll-heave data

The great interest of pitch-roll-heave data is that the comparisons between the model results and the observations can be carried out at different levels of complexity. Among the clearly identified paths are the significant wave height comparison, the mean wave direction comparison, and the frequency spectrum comparison. When selecting the tools we could have applied to the many results we had, we found it necessary to understand precisely some of them and define new ones. This is the aim of this section. It starts with a preliminary paragraph about the reduction of the various types of information (VAG model, WAM model, observations) to comparable quantities. These are gathered in a database from which all the comparisons are done, and to which all the tools further defined are applied. The three following paragraphs are devoted to the definition of tools for the comparisons of significant wave heights, of mean wave directions, and of spectra. The definition of the mean wave direction is adapted to take into account the limited directional information available from the data. In the last paragraph, some diagrams are designed to plot more directional information.

a. Preliminaries: a database

The buoy data consist of mean directions, $\Theta_{obs}(f_i)$, and energy densities, $E_{obs}(f_i)$, for 64 frequencies regularly spaced from 1/128 to 0.5 Hz, at irregular times, and describe the state of the sea at the location of the buoy. The models give a directional spectrum, $E_{mod}(f, \theta)$, for 12 (or 26) frequencies on a logarithmic scale, 12 (or 18) directions of propagation, every 6 hours, and at grid point locations. These characteristics have to be matched.

For each grid, the nearest point to the buoy location is selected (Table 2). The synoptic time (0000, 0600,

TABLE 2. Geographical collocation: for each grid, the nearest point to the buoy is given.

Grid			
Point location	stereo.150 km	stereo.100 km	1° × 1°
Distance	48°21′N, 5°43′W	48°18′N, 6°20′W	48°N, 6°W
from buoy	21 km	45.3 km	59 km

1200, and 1800 UTC) is attributed to the nearest observation with the restriction that the separation time is less than one hour. From the model outputs and the buoy records, 90 events are selected. Quantities computable from both model and buoy are defined. They consist of the energy densities $E(f_m)$ and the mean wave directions $\theta(f_m)$, for each frequency f_m on the frequency scale of the model VAG. The numerical schemes used to derive these quantities from the data and the models outputs are given in appendix A.

b. For the comparison of significant wave heights

The significant wave height H_s is obtained from the total energy E_T by

$$H_s = 4(E_T)^{1/2} \tag{5.1}$$

with

$$E_T = \sum E(f_m)\Delta f_m. \tag{5.2}$$

For the comparisons, the following statistical parameters are introduced:

- The *mean error* μ_H

$$\mu_H = [\sum (H_{\text{mod}} - H_{\text{obs}})]/N. \tag{5.3}$$

- The *standard deviation of the error* σ_H

$$\sigma_H = \{[\sum (H_{\text{mod}} - H_{\text{obs}} - \mu_H)^2]/(N-1)\}^{1/2}. \tag{5.4}$$

- The *scatter index* ϵ_H

$$\epsilon_H = \sigma_H/\mu_{H_{\text{obs}}}, \tag{5.5}$$

where $\mu_{H_{\text{obs}}}$ is the mean of the observations

$$\mu_{H_{\text{obs}}} = (\sum H_{\text{obs}})/N. \tag{5.6}$$

This scatter index is commonly used to quantify wave model performances, but is found to be not as relevant as expected. This point is developed in the analysis of the results.

The relative error is introduced, as it is another way to measure precision, and additive parameters are defined:

- The *mean* relative error $\mu_H{}^r$

$$\mu_H{}^r = [\sum (H_{\text{mod}} - H_{\text{obs}})/H_{\text{obs}}]/N. \tag{5.7}$$

- The *standard deviation of the relative error* $\sigma_H{}^r$

$$\sigma_H{}^r = \langle\{\sum [(H_{\text{mod}} - H_{\text{obs}})/H_{\text{obs}} - \mu_H{}^r]\}/(N-1)\rangle^{1/2}. \tag{5.8}$$

c. Comparison of mean wave directions

Usually, the mean wave direction, θ_M, is defined from the two-dimensional spectrum by

$$\theta_M = \arg\left[\int\int E(f,\theta)\exp(i\theta)dfd\theta\right] \tag{5.9}$$

but the data only provide the two quantities $\theta(f)$ and $E(f)$, related to the two-dimensional spectrum by (3.5) and

$$E(f) = \int E(f,\theta)d\theta \tag{5.10}$$

which cannot lead to the expression (5.9), as a simple application of the triangular inequality. So we decide to modify the definition in the form

$$\theta_M = \arg\left[\int E(f)\exp[i\theta(f)]df\right] \tag{5.11}$$

with $\theta(f)$ given by (3.5). This definition applies directly, both to the model outputs and the buoy data and does not necessitate any additional assumptions (as for example the shape of the observed spectrum). During the test period significant differences have been observed between the values obtained by (5.11) and those given by (5.9); an example is given in Fig. 2.

The following statistical parameters are defined:

- The *mean angular gap* μ_A

$$\mu_A = [\sum \Delta_{\text{ang}}]/N, \tag{5.12}$$

where Δ_{ang} is the angular gap between the observed and modeled mean wave directions, and the *weighted mean angular gap* μ_{WA}, which we define following the for-

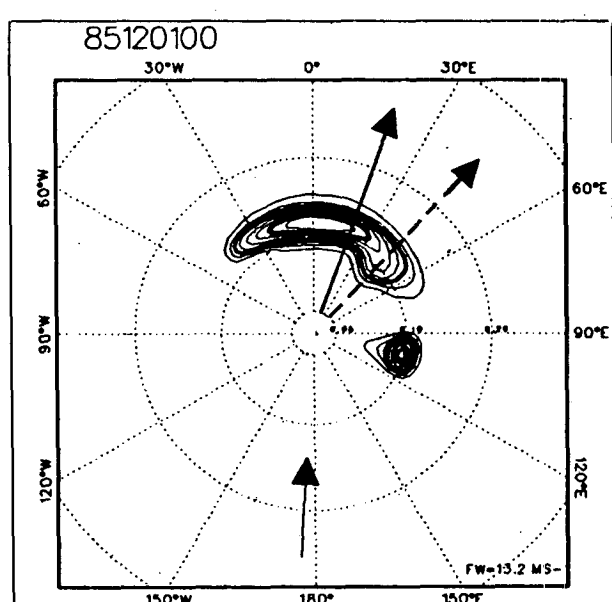

FIG. 2. Mean wave direction of a two-dimensional spectra obtained by VAGG2. The arrow toward the center gives the wind direction, the two others give the mean wave direction from (5.9) (regular arrow), and from (5.11) (dashed arrow).

mulation given by Audoin et al. (1987) for winds. These authors propose a weighting of the angular gap by the mean value of the observed and modeled wind speed. Since the aim of the present study is the comparison of results of several models, the interpretation is easier with a coefficient independent of the model. We suggest the use of the observed parameter only and the following definition:

$$\mu_{WA} = [\sum (H_{\text{obs}} \cdot \Delta_{\text{ang}})] / \sum H_{\text{obs}}]. \quad (5.13)$$

d. An adjustment criterion for the comparison of frequency spectra

Summarizing a great number of spectrum comparisons is not an easy task on the basis of numerous plots of observed and modeled spectra. Within the theoretical background of the stationary random processes applied to waves (Pierson 1955; Neumann-Pierson 1966; Borgman 1972), the statistical properties of the spectral estimates obtained from such a buoy are known and commonly used, as for example, to clarify the interpretation of the comparison diagrams with the adjunction of the limits of a confidence interval. To our knowledge, these statistical properties are not used to compare a great number of spectra. An adjustment criterion that may lead to practical interpretation for such studies is proposed. It is based on the statistical properties of the spectral estimates $E_{\text{obs}}(f_m)$ obtained from the buoy, namely the chi-square distribution of the quantities $2\nu E_{\text{obs}}(f_m)/E(f_m)$ for each frequency f_m of the frequency scale of the database. $E(f_m)$ is the spectrum value in term of stochastic process and ν the number of degrees of freedom. The determination of the parameter ν in the present case is given in appendix B. It is based on the hypothesis that within a frequency bin of the model, the true spectrum is slowly varying. With this statistical background, the usual procedure is to compute the limits of a 90% confidence interval for each estimate, and determine whether or not the model value falls within it. Using the same ideas in a slightly different way, it is possible to define a continuous criterion, which is more flexible. This is the aim of the next paragraph.

Since for each frequency the density function of $\eta = 2\nu E_{\text{obs}}(f_m)/E(f_m)$ is known, the probability p for η to range between any two values η_1 and η_2 is known. We suggest choosing these two values in such a way that p gives the probability for the true spectrum E to be less than α% of the modeled spectrum [i.e., range between $E_{\text{mod}}(f_m)(1-\alpha)$ and $E_{\text{mod}}(f_m)(1+\alpha)$], where α is a percentage to be chosen:

$$\eta_1 = 2\nu E_{\text{obs}}(f_m)/E_{\text{mod}}(f_m)(1+\alpha)$$

and

$$\eta_2 = 2\nu E_{\text{obs}}(f_m)/E_{\text{mod}}(f_m)(1-\alpha) \quad (5.14)$$

and lead to a criterion $p_\alpha(f_m)$ defined as being this probability. This criterion ranges from 0 to 1. With the first approximation that the instrumental errors are negligible compared with the model ones, it quantifies the ability of the modeled spectrum to be the true wave spectrum. For each comparison of observed and modeled spectra, it gives a frequency dependent criterion. Some properties of this criterion are more extensively described in the analysis of the results.

To interpret this criterion on the whole period, its mean value $\mu^{\alpha}_{FS}(f_m)$ and its standard deviation $\sigma^{\alpha}_{FS}(f_m)$ are computed for each frequency f_m. For convenience, when $E_{\text{mod}}(f_m)$ is zero, the value of $p_\alpha(f_m)$ is arbitrarily set to zero, and is discarded from any determination of mean and standard deviation value. When no events are kept for these determinations the two are also set to zero.

a. Some diagrams for the comparison of directional information

Some more information related to the directional aspects can be visualized, as shown for example by Ezraty (1981) with diagrams that gather arrows with direction $\theta(f_m)$ and length $E(f_m)/E_{\max}$ ($E_{\max}$ being the maximum value of the spectrum), for all the frequencies and versus time. Some modifications are proposed here to take into account the specific characteristics of the results and to improve their adequacy to the present comparison objectives: 1) $E(f_m)$ is replaced by $E(f_m)\Delta f_m$ which, in the case of a logarithmic scale for frequencies, gives a clearer understanding of the contribution of the wave of frequency f_m to the total energy. 2) Instead of using a normalization by $E_{\max}$ to prevent the length of the arrows from varying too much, a change of scale is done by setting this length to

$$h(f_m) = 4(E(f_m)\Delta f_m)^{1/2} \quad (5.15)$$

which represents, in a wave height equivalent, the contribution of the wave of frequency f_m to the total energy. It varies by the same order of magnitude as the significant wave height. It is thus more adapted to comparisons. Plots of arrows of direction $\theta(f_m)$ and length $h(f_m)$ are proposed. Only a few different times can appear on the same diagram. We also present, for a given frequency f_m, time series diagrams of $h(f_m)$ and $\theta(f_m)$. They are to be compared with those of significant wave height and mean wave direction previously described.

6. The results

The analysis of the results obtained with the various models starts with a qualitative interpretation of the time series diagrams of significant wave heights and mean wave directions, for three representative runs, VAG12, VAGG2 and WAM. A statistical study for all the runs follows, based on the values of the parameters defined previously. Frequency spectra are compared and the behavior of the adjustment criterion defined in section 5d is investigated. Complementary results

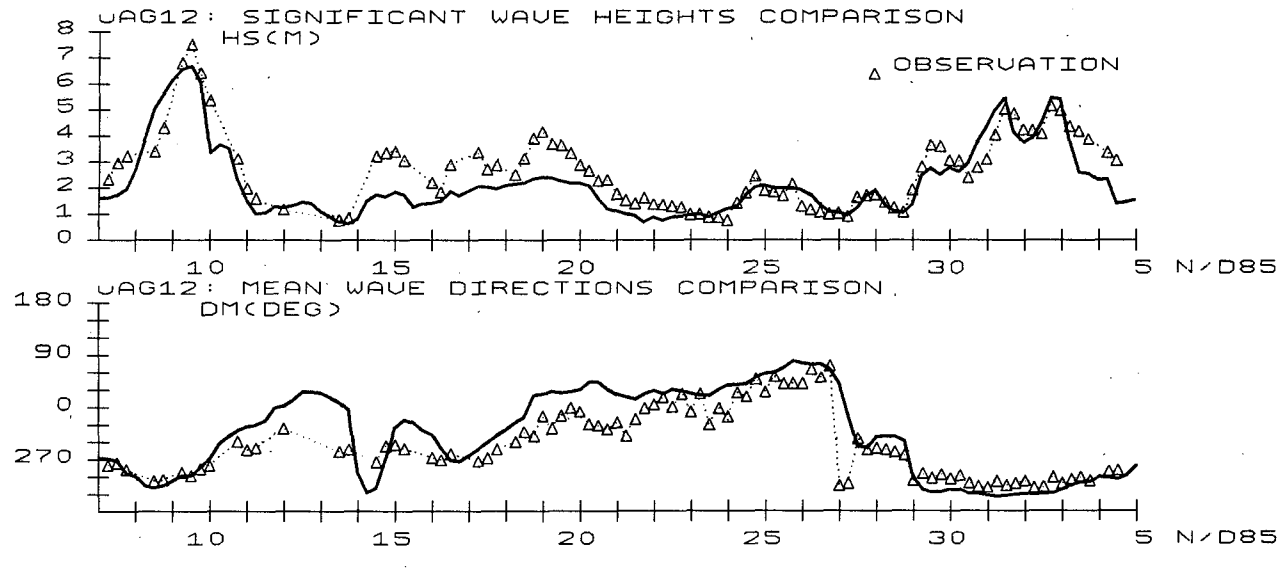
WAG12: SIGNIFICANT WAVE HEIGHTS COMPARISON
HS(M)
OBSERVATION
0
1
2
3
4
5
6
7
8
10
15
20
25
30
5
N/D85
WAG12: MEAN WAVE DIRECTIONS COMPARISON
DM(DEG)
180
90
0
270
10
15
20
25
30
5
N/D85

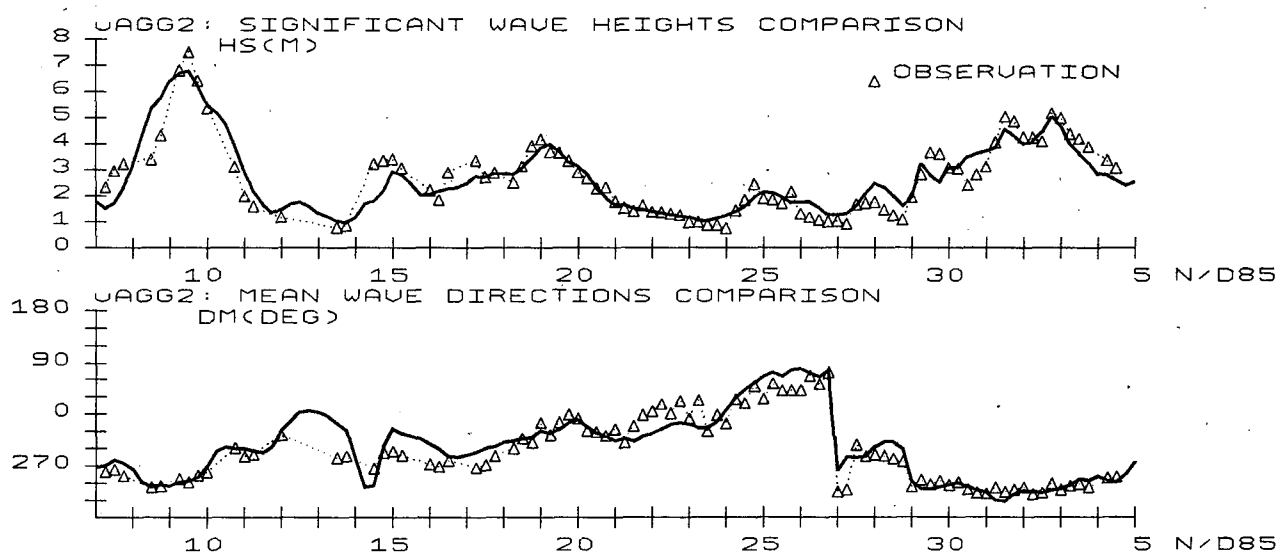
WAGG2: SIGNIFICANT WAVE HEIGHTS COMPARISON
HS(M)
OBSERVATION
0
1
2
3
4
5
6
7
8
10
15
20
25
30
5
N/D85
WAGG2: MEAN WAVE DIRECTIONS COMPARISON
DM(DEG)
180
90
0
270
10
15
20
25
30
5
N/D85

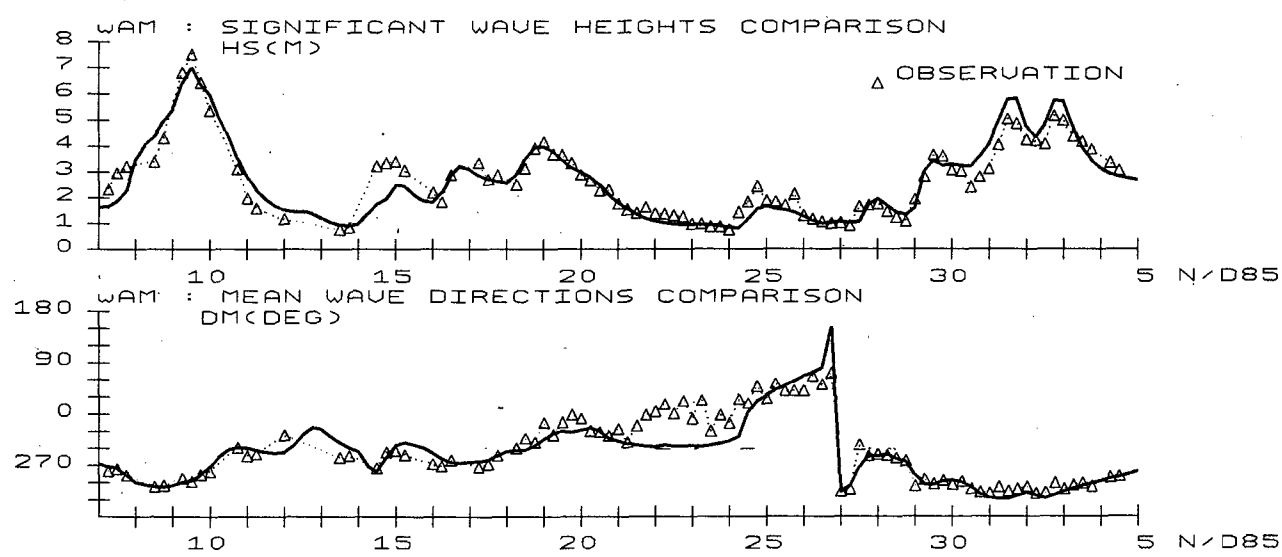
WAM : SIGNIFICANT WAVE HEIGHTS COMPARISON
HS(M)
OBSERVATION
0
1
2
3
4
5
6
7
8
10
15
20
25
30
5
N/D85
WAM : MEAN WAVE DIRECTIONS COMPARISON
DM(DEG)
180
90
0
270
10
15
20
25
30
5
N/D85

on directional aspects are discussed with the support of the diagrams presented in section 5e. The main results are summarized in the last paragraph.

a. Significant wave heights and mean wave directions comparisons

Plots of the time series of significant wave heights and mean wave directions for the three runs VAG12, VAGG2, and WAM, together with the observed values are presented in Fig. 3. It is clear that with both a coarse resolution in direction for the spectra, and in mesh size for the grid, VAG12 only partially describes the observations. Better results are obtained with VAGG2 and WAM. More precisely, three main periods are highlighted:

- A first storm at the beginning of November rises the significant wave height up to 7.5 m. The peak is well timed but underestimated by all runs. A plateau in the growth is only depicted by WAM. The decay is correctly described by VAGG2 and WAM.
- A second stormy situation with a double peak structure occurs at the end of the period. The timing of the peaks is correct but their intensities are differently modeled and seem to be slightly affected by grid modifications, as confirmed by the other runs. The mean wave directions are mainly steady and well reproduced.
- In between, a medium to low sea state is characterized by a trend in the mean wave directions, veering from west to east. This trend is correctly reproduced by VAGG2. For WAM, even though the wave heights are very well modeled, differences up to 80° happen (21 to 24 November). The sudden change in the mean wave direction on the 27 November is depicted by all runs.

A comparison of the observed wind, at the signal station of Ushant (48°28′N, 5°8′W) and of the ECMWF analyzed wind used by the models at the buoy grid point is given in Fig. 4. The high variability of the observations, probably because of the location of the wind sensor, on top of a cliff on the island, and because of the short time averaging (10 min) arouses suspicion on the relevance of these observations to drive any comparison. Referring to the quality of the ECMWF atmospheric model (Lange et al. 1987), and supported by the quality of the wave data (Racape 1987), investigations are thus restricted to the understanding of the differences that have appeared in the different runs and to their quantification, and this starts with the selection of useful parameters to highlight them.

From the values of the statistical parameters defined in sections 5b and 5c gathered in Table 3, what can be deduced?

For the significant wave height: the values of the mean error μ_H and of the mean relative error $\mu_H{}^r$ show that, except for VAG12, the biases are low and of the same order of magnitude. The scatter indexes ϵ_H are also of the same order of magnitude. All VAG runs have a 25% value for the standard deviation of the relative error, which is only 19% for WAM. It is interesting to compare more precisely the variability of the scatter index with that of the standard deviation of the relative error $\sigma_H{}^r$: 1) VAG12 has a scatter index higher than the other VAG runs but it does not lead to a higher value for the standard deviation of the relative error. This can be explained by the fact that the underestimation of wave heights occur to the highest waves (Fig. 3). Thus, the standard deviation of the error is high, as reflected by the scatter index, but this is not the case for that of the relative error. 2) On the other hand, WAM has a scatter index very near to the other VAG runs, although it shows a lower value for the standard deviation of the relative error. This mainly comes from the differences in the modeling of the low waves (Fig. 3) for which few centimeters are noticeable in terms of percentage. These remarks show that the scatter index has to be cautiously handled, because its definition mixes up two different aspects of data comparison: although it is expressed in percentage, it is the standard deviation of the error that is involved in its calculation and this does not give information about the relative error. Another shortcoming of the scatter index is its dependence on the mean value of the observations, which makes things very unclear while doing comparisons between results issued from different datasets (this is fortunately not the case here). This appears clearly in the following example: if, within a long period of time, a model and the observations perfectly agree except for a few days, the value of the scatter index (standard deviation of the error normalized by the mean of the observations) will depend on the absolute level reached outside the short period, as this level mostly determines the mean observation value, instead of only taking into account how good the agreement is outside this short period. We suggest the two evaluations in terms of error and relative error be done, as they elucidate different aspects of wave intensity adjustment, both of practical interest and of easy interpretation. In the present situation they show that 1) VAG12 underestimates the significant wave heights by 15% (−0.4 m), and mostly the highest ones. 2) All other runs have a similar and low bias (even if some bias is noted in one evaluation, it is not confirmed by the other one). 3) All VAG adjustments have a scatter of the same order of magnitude. It is lower for WAM, mainly because of a better prediction of the intensity of the lower waves. The two models have similar values

FIG. 3. Significant wave height and mean wave direction. Comparison with the buoy measurements (Δ· · ·) for the runs, VAG12, VAGG2, and WAM.

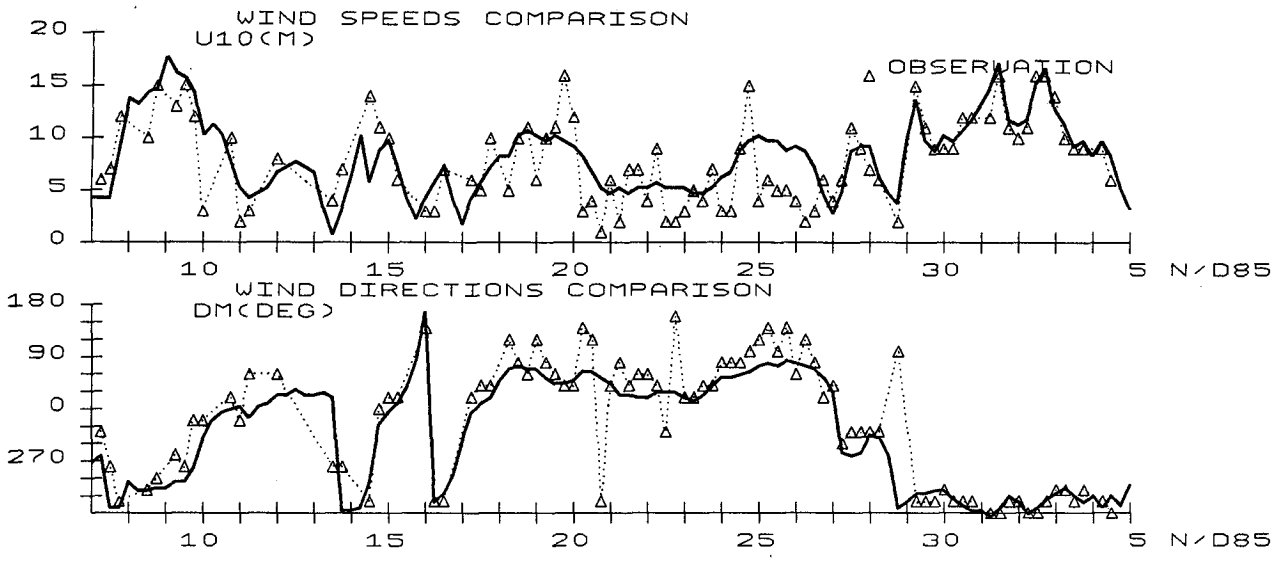

FIG. 4. Wind speed and direction. Comparison between the 10 m analyzed wind of the ECMWF archive used for all runs (——) and the observation of the signal station of Ushant (Δ· · ·).

for the mean angular gap μ_A and for the weighted mean angular gap μ_{WA}. The weighting by the significant wave height decreases the mean value by one fourth and shows that the direction of the higher waves is better predicted.

b. Frequency spectrum comparisons

Before presenting the results obtained with the different runs, some aspects of the new p_α-criterion defined in section 5d are described; e.g., its dependence on the frequency, the way it quantifies the "visual" discrepancy between two spectra, its dependence on α, and the validity of the hypotheses made.

1) SOME PROPERTIES OF THE p_α-CRITERION

To start with, plots of modeled and observed spectra together with their corresponding p_α-criterion values are prepared, for α = 10%, 20%, 30% and 40% (Figs. 5 and 6). The envelopes at 20% from the model spectrum are added (dotted line) in Fig. 5. By definition, for each frequency f, $p_{20\%}(f)$ is the probability for the true spectral value to be in the domain limited by these two curves. These diagrams help to understand some aspects of the behavior of the proposed adjustment criterion: 1) it is always zero for the lowest frequencies, as a consequence of zero energy in these frequency bins. 2) For the highest frequencies (Fig. 6), its values are rapidly decreasing and reflect that measurement errors are no longer negligible. 3) It is extremely rare that the criterion is steady on all the remaining frequency ranges, and it falls quickly to very low values as soon as the observed values diverge from the modeled spectrum (Fig. 5). This is outlined clearly in Fig. 7 where the values of the 20% criterion are plotted, for all frequencies and for the whole period, as function of $R = |E_{obs}(f_m)/E_{mod}(f_m) - 1|$. 4) An increase of the value of α (Fig. 6), increases the value of the criterion (which is not surprising) and keeps the main features of the frequency dependence. This is also ver-

TABLE 3. Significant wave heights and mean wave directions comparison. Here μ_H is the mean and σ_H the standard deviation of the error, $\mu_H{}^r$ is the mean and $\sigma_H{}^r$ the standard deviation of the relative error, ϵ_H is the scatter index, μ_A is the mean angular gap, and μ_{WA} the weighted mean angular gap. The μ_H and σ_H are in meters and μ_A and μ_{WA} are in degrees.

	Significant wave height			Mean wave direction	
MODEL	μ_H (σ_H)	$\mu_K{}^r$ ($\sigma_H{}^r$)	ϵ_H	μ_A	μ_{WA}
VAG12	−.42 (.73)	−14% (26%)	.27	28.6	24.1
VAG18	+.02 (.59)	+6% (25%)	.22	16.7	12.7
VAGAD1	−.15 (.62)	−1% (25%)	.23	17.5	14.0
VAGDO	+.10 (.61)	+9% (26%)	.23	16.7	12.4
VAGG2	.00 (.56)	+5% (24%)	.21	15.8	12.4
WAM	−.02 (.51)	−1.5% (19%)	.19	16.6	11.9

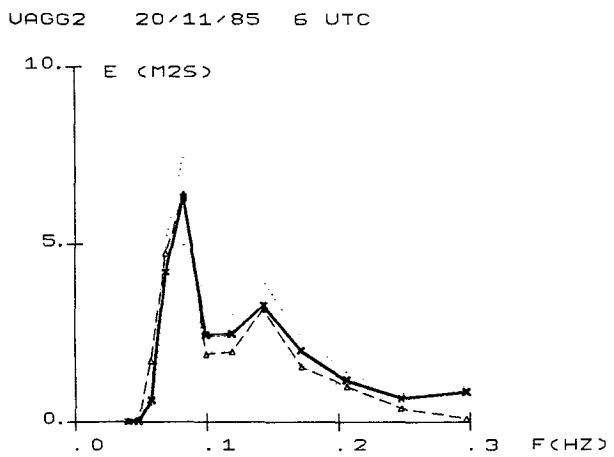

FIG. 5. Frequency spectra comparison: (Δ---) buoy, (——) model, (· · ·) envelopes at 20% from the model spectrum.

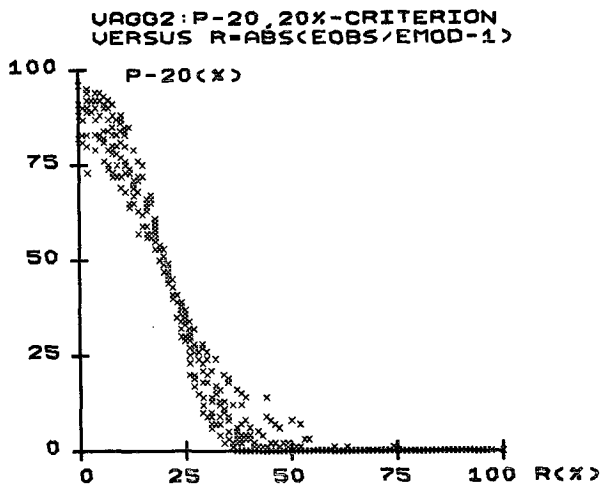

FIG. 7. The 20%-adjustment criterion as a function of $|E_{obs}(f_m)/E_{mod}(f_m) - 1|$, for all frequencies f_m, and for the whole period 7 November–5 December 1985 (run VAGG2). The value of the criterion falls quickly to zero as soon as the observed spectral value diverges from the modeled one.

ified for the mean and the standard deviation, thus we only present them for $\alpha = 20\%$ (Figs. 8–11). This value of α agrees roughly with a 10% error for the significant wave height.

A first investigation of sampling variability effects has been done by preparing the same plots on subsets of the database; e.g., the first half period, with significant wave heights higher than three meters. Some differences appear but they do not contradict the results below.

The validity of the hypothesis of a slow variation of the spectrum in frequency and its impact on the calculation of the criterion has been tested. The initial discretization of the spectra of the WAM model in 26 frequencies makes possible the determination of the criterion on less averaged spectra estimates. The mean value and standard deviation thus obtained are compared with the previous ones in Figs. 12 and 13. The scatter is slightly lower, but the level and the variations of the mean are very similar, with however an accentuation of a break between high and low frequencies.

2) USE OF THE p_α-CRITERION FOR THE COMPARISON OF SPECTRA

Some interpretations based on the values of the mean of the $p_{20\%}$-criterion on the whole period are now presented, starting with the model VAG. Figure 8 shows that VAG12 fails in the modeling of swell (low frequencies), that decreasing the angular discretization to 20° (VAG18) is favorable, but that the benefit is lost when the propagation scheme is reduced to a first

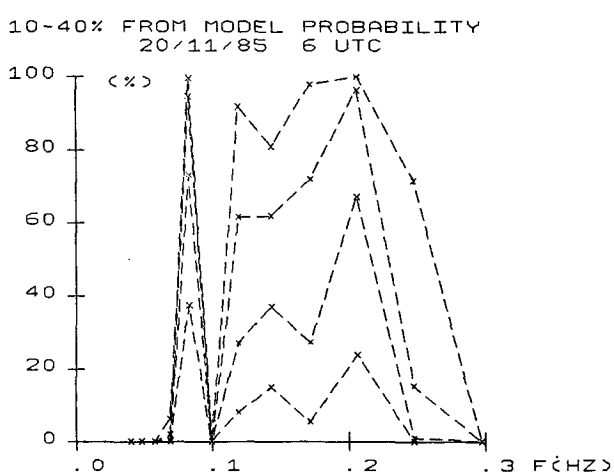

FIG. 6. Frequency spectra comparison: adjustment criterion p_α corresponding to the spectra of Fig. 5, for $\alpha = 10\%$, 20%, 30%, and 40% (from bottom to top).

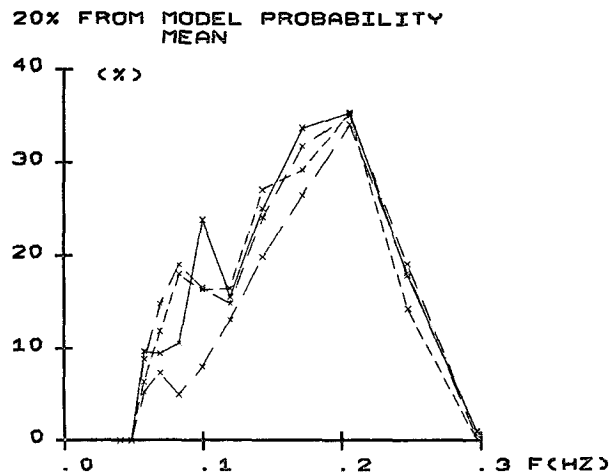

FIG. 8. Frequency spectra comparison: mean value of the 20%-adjustment criterion over the period 7 November–5 December 1985: (– – –) VAG12, (——) VAGAD1, (---) VAGG2, and (– · –) VAG18.

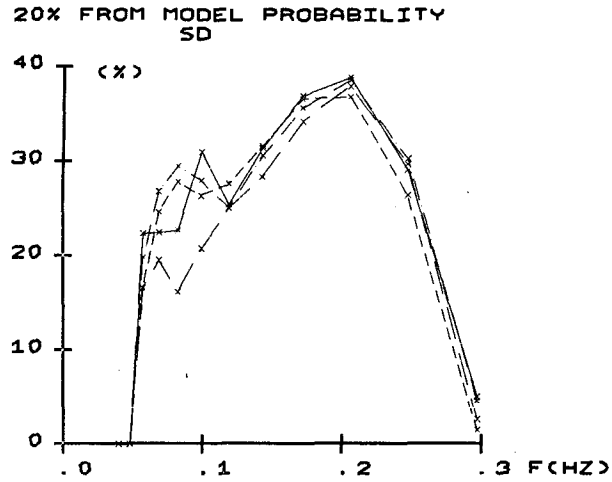

FIG. 9. Frequency spectra comparison: standard deviation of the 20%-adjustment criterion over the period 7 November–5 December 1985:(- - -) VAG12, (——) VAGAD1, (---) VAGG2, (-·-) VAG18.

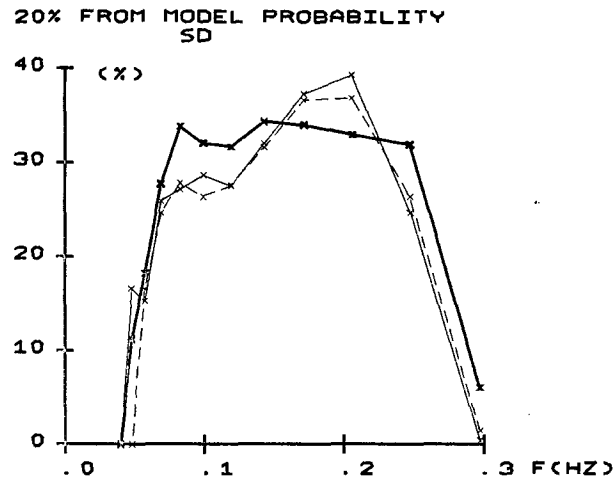

FIG. 11. Frequency spectra comparison: standard deviation of the 20%-adjustment criterion over the period 7 November–5 December 1985: (---) VAGG2, (——) VAGDO, (▬) WAM.

order (VAGAD1). The sudden increase in this case for f_m around 0.1 Hz is of no meaning as the standard deviation (Fig. 9) is also increased. Decreasing the mesh size to 100 km (VAGG2) does not bring noticeable improvement. The reshaping of the windsea according to the parameterization of Donelan et al. (1985), leads to a better adjustment for the high frequencies (VAGDO, Fig. 10). This is consistent with the conclusions of these authors that the rear face of the spectrum is better described with a f^{-4} power law.

For WAM, the mean quality of the adjustment appears as mainly steady on the whole frequency range (Fig. 10). Swells are better modeled. However, for high frequencies, WAM does not give as good results as VAG with the parameterization of Donelan (VAGDO) or even with the JONSWAP parameterization (VAGG2).

For all the runs, a break appears in the mean value between high and low frequencies. It is very tempting to attribute this decrease to shortcomings in the modeling of the interactions between swell and windsea, because it is mainly at these frequencies that they happen. However, these conclusions have to be tempered by the fact that the scatter is important (Figs. 9 and 11). This scatter outlines how much has to be done to reach the true spectrum modeling.

c. *Directional aspects*

In this section, the comparisons between models and observations are carried on with the support of the full

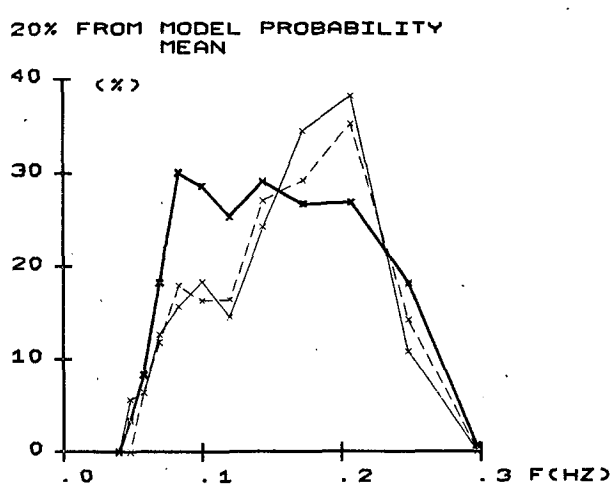

FIG. 10. Frequency spectra comparison: mean value of the 20%-adjustment criterion over the period 7 November–5 December 1985: (---) VAGG2, (——) VAGDO, (▬) WAM.

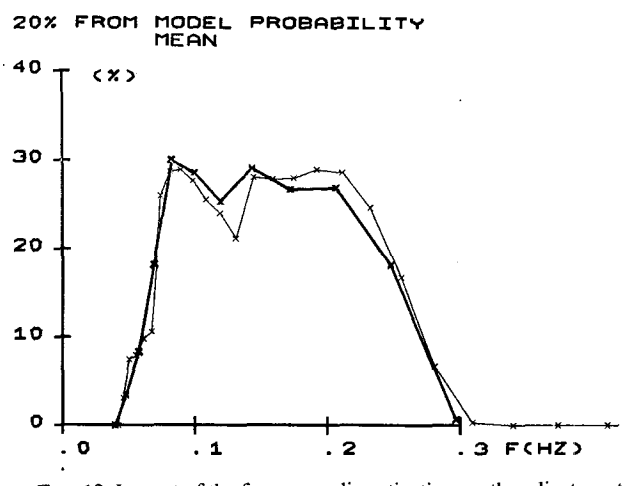

FIG. 12. Impact of the frequency discretization on the adjustment criterion: mean value of the 20%-adjustment criterion over the period 7 November–5 December 1985: (▬) WAM 12 frequencies, (——) WAM 26 frequencies.

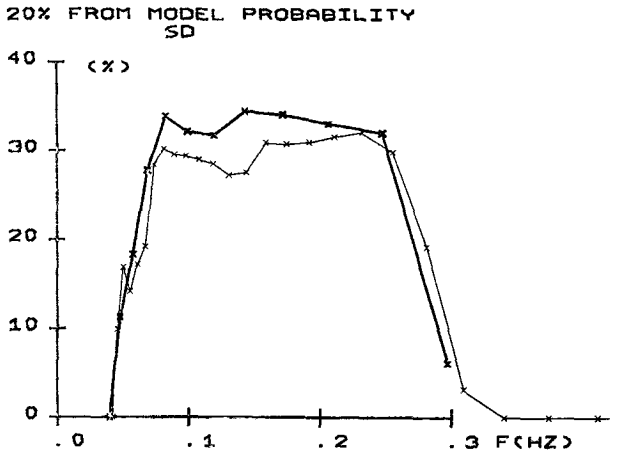

FIG. 13. Impact of the frequency discretization on the adjustment criterion: standard deviation of the 20%-adjustment criterion over the period 7 November–5 December 1985: (——) WAM 12 frequencies, (——) WAM 26 frequencies.

database, emphasizing the directional aspects. In Figs. 14 and 15 this information is plotted for WAM and VAGG2, in comparison with the observed values, for 26 and 27 November. During these two days, although the wave heights are low, their spectral structure is complex, due to a sudden change in the wind direction, backing from east-northeast to west-northwest, and to a superimposed westerly swell. This swell (bottom of the diagrams) is similarly described in intensity by the two models. VAGG2 gives it from the west and WAM from the west-southwest which is nearer to the observations. Looking at the windsea (top of the diagrams), one can see that after the changing of wind direction (27 at 0 h), VAGG2 adjusts more quickly to the observed wave direction, and that WAM shows a lag time. To investigate this point, the evolution of the energy (in terms of wave height equivalent) and of the mean wave direction has been prepared for various frequencies. It is given, with the wind direction added in dashed line, for f_m = 0.17 Hz in Fig. 16. Whenever the wind direction changes, the data show a lag time between wind turning and wave turning. This lag time is correctly reproduced by VAGG2 but is too long with WAM. A shift tendency of the mean direction towards the swell direction is also outlined (21 to 24 November) in the case of this model. Figures 14 and 15 also show that the separation between windsea and swell is around 0.1 Hz, the frequency around which a reduction in the criterion mean value has previously been noticed (Figs. 10 and 12). The evolution of the mean direction for the nearest frequency to this value (f_m = 0.12 Hz) is thus of interest and is given in Fig. 17. When the mean wave direction is far from the wind direction, and waves are then swell dominated, WAM gives better results, but as soon as this direction is nearer to the wind di-

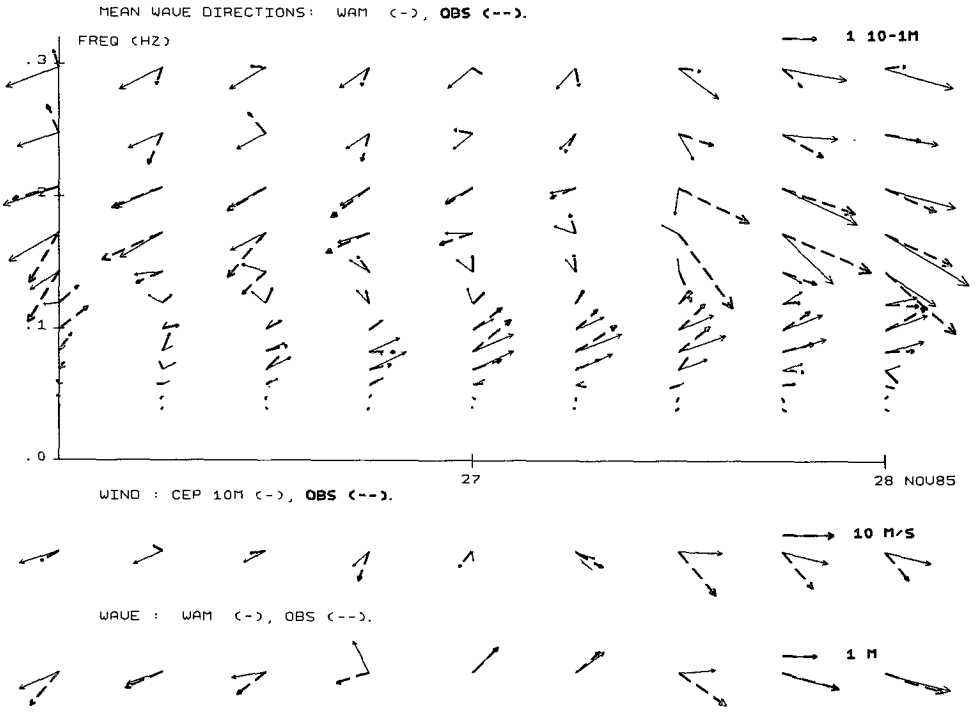

FIG. 14. Full information plotting. Comparison between buoy and WAM for 26 and 27 November. For each frequency f_m, an arrow of direction $\theta(f_m)$ (north to the top), and length $h(f_m) = 4\langle E(f_m)\rangle^{1/2}$ is plotted.

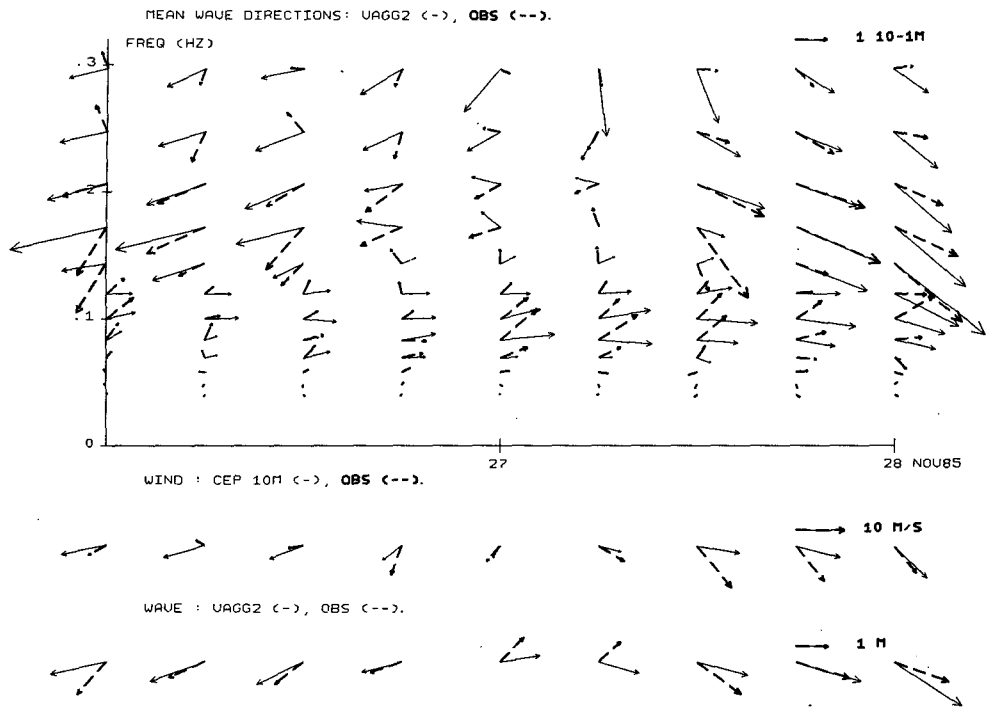

FIG. 15. Full information plotting. Comparison between buoy and VAGG2 for 26 and 27 November. For each frequency f_m, an arrow of direction $\theta(f_m)$ (north to the top), and length $h(f_m) = 4\langle E(f_m)\rangle^{1/2}$ is plotted.

rection, and waves are then windsea dominated, VAGG2 behaves better—again even in wind turning situations.

d. Summary of the main results

The significant wave height and mean wave direction comparisons show that in the mean VAG and WAM achieve similar results, except for the relative error, for which WAM shows a lower scatter. The new criterion defined for the comparison of frequency spectra highlights that for VAG a reshaping of the windsea with a f^{-4} power law is better than a f^{-5} one for the high frequency tail of the spectrum. It also shows that the swell modeling is improved by reducing the directional resolution of the spectrum to 20 degrees. Swells are better obtained with WAM. This model uses a first order propagation scheme and a 30 degree resolution for the spectrum, but, with a 1 degree × 1 degree resolution for the grid, has a much higher resolution in the west–east direction from where most of the swells are coming and takes into account the Irish coast better. To further decide the relative impact of the coastal setup in the model and of the propagation schemes, observations in the open ocean are crucial. A final study on the directional behaviors of the two models shows that, in wind turning situations, a lag time between wind turning and wave turning is observed by the buoy even for rather high frequency waves. This lag time is correctly reproduced with VAG, but is too long with WAM.

7. Conclusion

A one month hindcast on November 1985 has been done with five versions of the second generation model VAG and with the version WAMD1 of the third generation model WAM. The same windfields from the ECMWF archive are used and the results are compared with the data from the pitch–roll–heave sensor of the buoy "BEATRICE" moored at the entrance of the channel by 110 meters depth.

The comparisons start with the study of the significant wave heights and of the mean wave directions.

For the significant wave height comparisons, the notions of error and relative error are used, as they clarify well-defined aspects of adjustment quality, both having practical interpretation. It is outlined that this is not the case for the scatter index, especially while doing comparisons over long periods or with various datasets. It is shown that on the basis of classical statistical tests WAM and VAG achieve similar results. The introduction of the relative error highlights a lower scatter for WAM.

For the mean wave directions it is first pointed out that its definition needs to be adapted to take into account the specific characteristics of the pitch–roll–heave

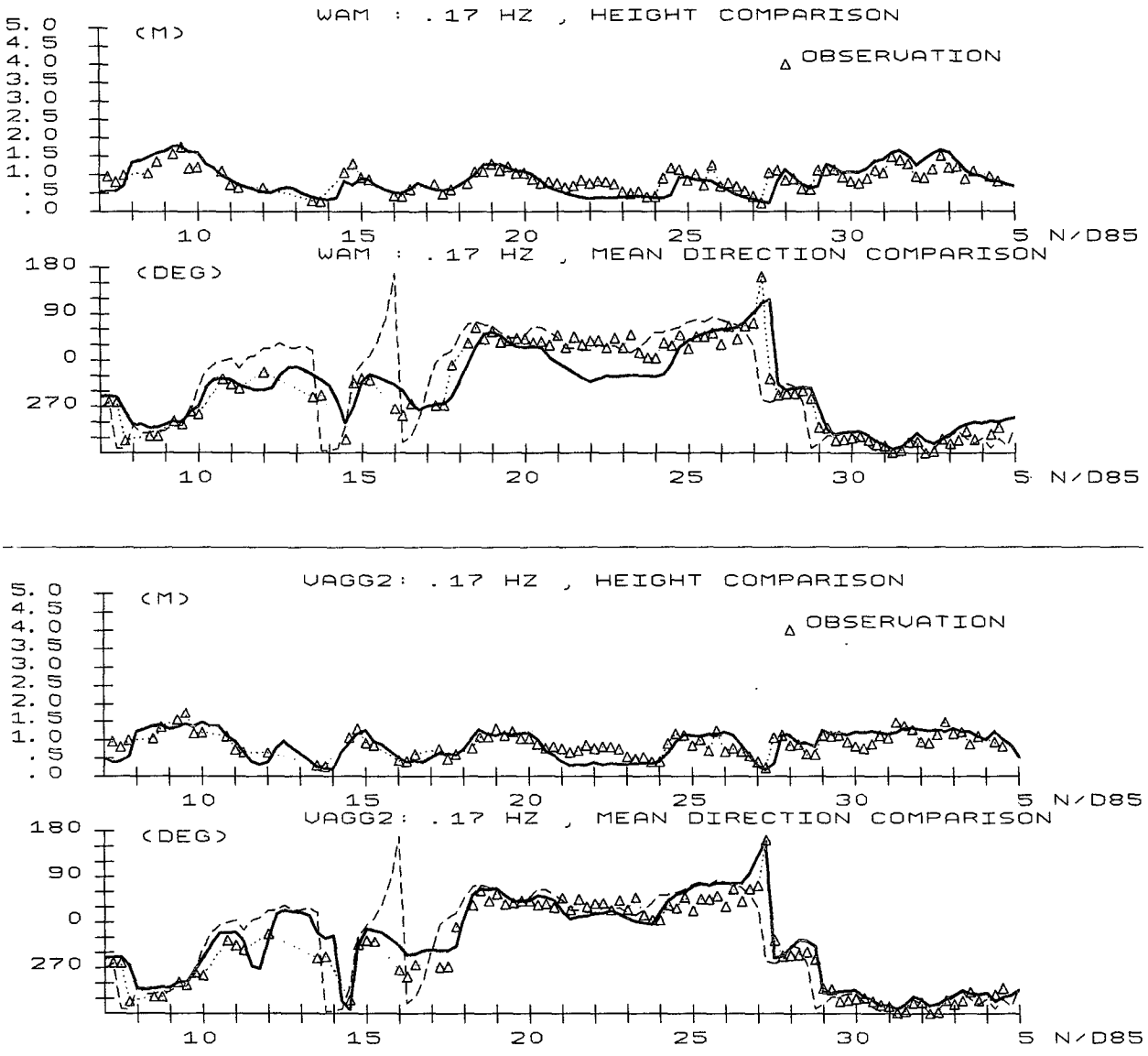

FIG. 16. Energy, in term of height equivalent $h(f_m)$, and mean direction for the frequency bin centered in $f_m = 0.17$ Hz. Comparison with the buoy data ($\Delta \cdots$) for WAM and VAGG2. The direction of the wind used by the models is added in dashed line.

data and avoid making additional assumptions on the shape of the spectrum. The values of a weighted mean angular gap minimizing the influence of the direction errors of the low waves outline that higher waves are better reproduced. No new differences between the various runs are discovered. This shows the limitations, to further investigate the behavior of wave models, of existing standard statistical tests based on the only comparison of significant wave heights and mean wave directions.

The next step is the comparison of the frequency spectra. An adjustment criterion is defined to quantify in terms of probability, the ability of the model to give the true spectrum. Some tests with this criterion are reported and used to illustrate some of its properties. Its application to the various model runs has highlighted differences that were previously indiscernible: 1) in VAG, a reshaping of the windsea with an f^{-4} power law for the rear face of the spectrum is better than an f^{-5} one; 2) the swell modeling is improved by reducing the directional resolution of the spectrum; 3) swells are better modeled with WAM.

Finally, some diagrams are designed to present more of the directional aspects. They show that, in wind turning situations, a lag time between wind turning and wave turning is observed by the buoy even for rather high frequency waves. This lag time is correctly reproduced with VAG, but is too long with WAM.

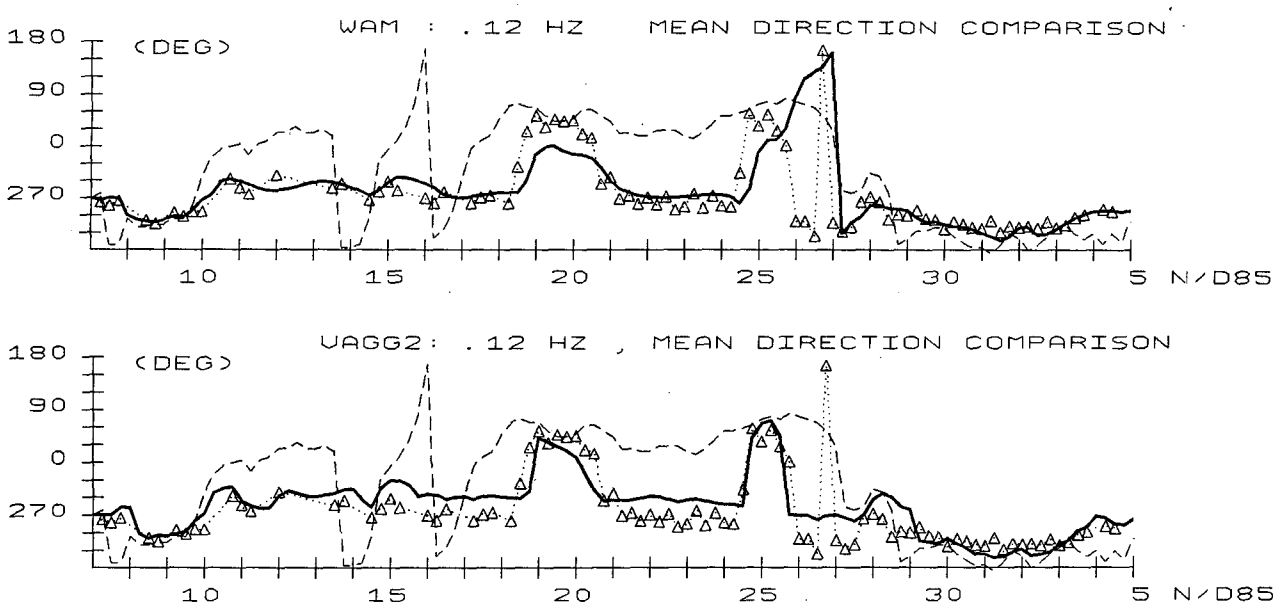

FIG. 17. Mean direction for the frequency bin centered in 0.12 Hz. Comparison with the buoy data ($\Delta\cdots$) for WAM and VAGG2. The direction of the wind used by the models is added in dashed line.

Acknowledgments. I am indebted to the "Service Technique des Phares et Balises" which has provided the data, and thank J. F. Racape and L. Schmiedt for useful discussions. The run with the WAM model was done at the European Centre for Medium Range Weather Forecasts, and supported by the European Community, as part of a stimulation action for European scientific cooperation ST2J-0044-10-F.

APPENDIX A

Determination of the Database

The values included in the database are the energy densities $E(f_m)$ and the mean wave directions $\theta(f_m)$, for each frequency f_m on the frequency scale of the model VAG, which are the most informative quantities jointly computable from the models outputs and the buoy data.

From the VAG spectral outputs, they are obtained by integration:

$$E(f_m) = \sum E(f_m, \theta)\Delta\theta \qquad \text{(A.1)}$$

and

$$\theta(f_m) = \arg\Big(\sum E(f_m, \theta)\exp(i\theta)\Delta\theta\Big). \qquad \text{(A.2)}$$

From the buoy data, an interpolation is necessary and one preserving the total energy is chosen. For a given frequency f_m, corresponding to a frequency bin, (f_{m_1}, f_{m_2}), the two indices i_1 and i_2 are calculated

$$(i_1 - 1.5)\Delta f \leqslant f_{m_1} \leqslant (i_1 - 0.5)\Delta f \quad \text{and}$$
$$(i_2 - 1.5)\Delta f \leqslant f_{m_2} \leqslant (i_2 - 0.5)\Delta f, \qquad \text{(A.3)}$$

where Δf is the frequency bandwidth of the data, $\Delta f = 1/128$. The energy density $E(f_m)$ for the frequency f_m is then obtained with the following formula:

$$E(f_m) = [1/(f_{m_2} - f_{m_1})]\{\sum \Delta f E_{\text{obs}}(i\Delta f) + [(i_1 - 0.5)\Delta f - f_{m_1}]E_{\text{obs}}[(i_1 - 1)\Delta f] + [f_{m_2} - (i_2 + 0.5)\Delta f]E_{\text{obs}}[(i_2 + 1)\Delta f\}, \quad i = i_1 \cdots i_2. \qquad \text{(A.4)}$$

The same weighting is applied to obtain the mean direction $\theta(f_m)$.

From the WAM spectral outputs, the mean energy densities and the mean wave directions are calculated by integration for the 26 frequencies, applying (A.1) and (A.2), and are then interpolated to 12 frequencies with a similar scheme as used in (A.4).

APPENDIX B

Statistical Properties of the Spectral Estimates Obtained from the Buoy

A single record of length T of the sea surface elevation, $\eta_r(t)$, $0 < t \leqslant T$, as given by the buoy, provides us with an estimate E_{obs} of the power spectrum E of the stochastic process $\eta(t)$.

The method starts with a fast Fourier transform of the digitized signal

$$\eta_r(0), \ldots, \eta_r[(N-1)\Delta t)] \qquad (N = 4096,\ \Delta t = 0.5 \text{ sec})$$

which gives the coefficients (a_n, b_n) of the following Fourier representation:

$$\eta_r(q\Delta t) = \sum a_n \cos(2\pi qn/N) + b_n \sin(2\pi qn\Delta t/N\Delta t), \quad n = 0, \cdots, N/2. \qquad \text{(B.1)}$$

As the mean elevation is the reference level, a_0 is zero, and without lost of generality, $b_{N/2}$ is set to zero. An estimate E_{es} of the true spectrum is then obtained by

$$E_{es}(f_n) = (a_n^2 + b_n^2)/2 \qquad \text{(B.2)}$$

for $f_n = f_0, \cdots, Nf_0/2$, where $f_0 = 1/T = 1/N\Delta t$.

For a Gaussian process the quantity, $2E_{es}(f_n)/E(f_n)$ is distributed as a chi square with two degrees of freedom (except for $n = 1$ and $N/2$, where it is one) and the estimates obtained with two different frequencies are independent. This is also approximately true for a non-Gaussian process as N is large (Jenkins and Watts 1969).

The spectrum is then smoothed by averaging over k equal to 16 adjacent estimates, which gives a new estimate E_{ess}. Under the hypothesis that the true spectrum is not too rapidly varying, each quantity $2kE_{ess}(f_n)/E(f_n), f_n = kf_0/2, 3kf_0/2, \cdots$ is distributed as a chi square with $2k$ degrees of freedom, and two estimates obtained for two different frequencies are independent as there is no overlapping of averaged frequency bands.

In (A.4) the interpolation made to obtain the spectral estimates for the database, E_{obs}, is done by weighted averaging. The scale being logarithmic, the number j of spectral values involved and the weight coefficients vary. This makes the presentation of the process more tedious. However, this choice of scale is made to obtain better resolution of the spectrum in the peak region and the hypothesis of a true spectrum slowly varying can reasonably apply. The quantities $2\nu E_{\text{obs}}(f_m)/E(f_m)$ are then distributed as a chi square with 2ν degrees of freedom, with $\nu = kj$ but two estimates obtained with different frequencies are no longer independent.

REFERENCES

Audoin, J. M., D. Rousseau and R. Juvanon du Vachat, 1987: Evaluation du modèle à maille fine PERIDOT, comparaison avec le modèle EMERAUDE. Note de travail de l'Etablissement d'Etudes et Recherches Météorologiques, No. 184, 11.

Barnett, T. P., 1968: On the generation, dissipation and prediction of ocean wind waves. *J. Geophys. Res.*, **73**, 513–529.

Borgmann, L. E., 1972: Confidence intervals for ocean wave spectra. *Proc. of the Thirteenth Coastal Engineering Conf.*, Vancouver, 237–250.

Donelan, M. A., J. Hamilton and W. H. Hui, 1985: Directional spectra of wind generated waves. *Phil. Trans. Roy. Soc. London*, **315**, 509–562.

Ezraty, R., and A. Cavanié, 1981: Evaluation de la mesure de la direction des vagues à partir des données d'une bouée instrumentée. *Oceanol. Acta*, **4**, 139–149.

——, —— and J. P. Gouillou, 1983: Système de mesures de houles directionnelles, CNEXO/COB-Rapport Scientifique et technique, No. 53.

Foristall, G. Z., 1981: Measurement of a saturated range in ocean wave spectra. *J. Geophys. Res.*, **86**, 8075–8084.

Gadd, 1978: A numerical advection scheme with small phase speed errors. *Quart. J. Roy. Meteor. Soc.*, **104**, 569–582.

Gelci, R., and E. Devillaz, 1969: Le calcul numérique de l'état de la mer. Note de travail de l'Etablissement d'Etudes et Recherches Météorologiques, No. 268.

Golding, B., 1983: A wave prediction system for real time sea state forecasting. *Quart. J. Roy. Meteor. Soc.*, **109**, 393–416.

Guillaume, A., 1987: VAG-Modèle de prévision de l'état de la mer en eau profonde. Note de travail de l'Etablissement d'Etudes et Recherches Météorologiques, No. 178.

Hasselmann, K., 1962: On the non-linear energy transfer in a gravity wave spectrum. 1: General theory. *J. Fluid Mech.*, **12**, 481–500.

——, T. P. Barnett, E. Bouws, H. Carlson, D. E. Catwright, K. Enke, J. A. Ewing, H. Gienapp, D. E. Hasselmann, P. Kruseman, A. Meerburg, P. Muler, D. J. Olbers, K. Richter, W. Sell and H. Walden, 1973: Measurements of wind-wave growth and swell decay during the Joint North Sea Wave Project (JONSWAP). *Dtsch. Hydrogr. Z.*, **8**.

——, 1974: On the spectral dissipation of ocean waves due to white capping. *Bound.-Layer Meteor.*, **6**, 107–127.

——, D. B. Ross, P. Muller and W. Sell, 1976: A parametric wave prediction model. *J. Phys. Oceanogr.*, **6**, 200–228.

Hasselmann, S., 1987: The WAM wave model system. Rep. Max-Planck-Institut fur Meteorologie, Hamburg.

——, and K. Hasselmann, 1985a: Computations and parameterizations of the nonlinear energy transfer in a gravity wave spectrum. Part 1: A new method for efficient computations of the exact nonlinear transfer integral. *J. Phys. Oceanogr.*, **15**, 1369–1377.

——, ——, J. H. Allender and T. P. Barnett, 1985b: Computations and parameterizations of the nonlinear energy transfer in a gravity wave spectrum. Part 2: Parameterizations of the nonlinear energy transfer for application in wave models. *J. Phys. Oceanogr.*, **15**, 1378–1391.

Jenkins, G. M., and D. G. Watts, 1969: *Spectral Analysis and Its Applications*. Holden Day, 525 pp.

Kitaigorodskii, S. A., V. P. Krasitskii and M. M. Zaslavskii, 1975: On Phillips' theory of an equilibrium range in the spectra of wind generated gravity waves. *J. Phys. Oceanogr.*, **5**, 410–420.

Komen, G. J., 1985: Activities of the WAM (Wave Modelling) group. *Advances in Underwater Technology*, Ocean Science and Offshore Engineering, Vol. 6, Graham and Trotman, 121–127.

Lange, A., and K. Tokkola, 1987: Results of the WMO/CAS NWP data study and intercomparison project for forecast for the Northern Hemisphere in 1986. WMO publication.

Longuet-Higgings, M. S., D. E. Cartwright and N. D. Smith, 1963: Observation of the directional spectrum of sea waves using the motion of a floating buoy. *Ocean Wave Spectra*, Prentice Hall, 111–136.

Mitsuyasu, H., F. Tasai, T. Suhara, S. Mizuno, M. Ohkusu, T. Honda and K. Rikiishi, 1975: Observations of the directional spectrum of ocean waves using a cloverleaf buoy. *J. Phys. Oceanogr.*, **5**, 750–760.

Neumann, G., and W. J. Pierson Jr., 1966: Probability, statistics and time series. *Principle of Physical Oceanography*, Prentice Hall, 480–493.

Pierson, W. J., Jr., 1955: Wind generated gravity waves. *Advances in Geophysics*, Vol. 2, Academic, 93–178.

——, and L. Moskowitz, 1964: A proposed spectral form for fully developed wind seas based on the similarity theory of S. A. Kitaigorodskii. *J. Geophys. Res.*, **69**, 5181–5190.

Racapé, J. F., and R. Ezraty, 1987: Mesures de comportement d'une bouée géante et évaluation du spectre directionnel de la houle à partir de ces mesures. R. Tech. du Service des Phares et Balises, No. 76.

Snyder, R. L., F. W. Dobson, J. A. Elliott and R. B. Long, 1981: Array measurements of atmospheric pressure fluctuations above surface gravity waves. *J. Fluid Mech.*, **102**, 1–59.

The SWAMP Group, 1985: Sea Wave Modelling Project (SWAMP). An intercomparison study of wind wave prediction models, Part 1: Principal results and conclusions. *Ocean Wave Modelling*, Plenum Press, 256 pp.

WAM-Development and Implementation Group, K. Hasselmann, E. Bauer, P. A. E. M. Jansen, G. J. Komen, L. Bertotti, P. Lionello, A. Guillaume, V. C. Cardone, J. A. Greenwood, M. Reistad, L. Zambresky and J. A. Ewing, 1988: The WAM model, a third generation ocean wave prediction model. *J. Phys. Oceanogr.*, **18**, 1775–1810.